Molecular Simulation of the Vapor-Liquid Phase Behavior of Cyanides and Their Binary Mixtures

Svetlana Miroshnichenko[1], Thomas Grützner[2], Daniel Staak[2], Jadran Vrabec[1] *

[1] Lehrstuhl für Thermodynamik und Energietechnik, Universität Paderborn, Warburger Straße 100, 33098 Paderborn, Germany

[2] Lonza AG, Chemical Research and Development, CH-3930 Visp, Switzerland

Keywords: Molecular modeling and simulation; vapor-liquid equilibrium; Cyanogen; Cyanogen chloride; Hydrogen cyanide; Acetonitrile

Abstract

The vapor-liquid phase behavior of binary mixtures containing Cyanogen, Cyanogen chloride, Hydrogen cyanide and Acetonitrile is predicted by molecular simulation and compared to experimental data as well as the Peng-Robinson equation of state. Two new molecular force field models are presented for Cyanogen and Cyanogen chloride, molecular models for the other compounds are taken from preceding work. The parametrization of the present classical molecular interaction models is carried out on the basis of quantum chemical calculations and subsequent fitting to experimental vapor pressure and saturated liquid density data. To validate the present molecular models, vapor-liquid equilibria for the pure cyanides and 14 binary mixtures containing cyanides are calculated and compared with the available experimental data and the Peng-Robinson equation of state. In general, the simulation results are in good agreement with the experimental data.

* corresponding author, tel.: +49-5251/60-2421, fax: +49-5251/60-3522, email: jadran.vrabec@upb.de

1 Introduction

Cyanides are chemical compounds that contain the cyano group N≡C-R. Solutions of cyanides readily bond with gold, silver and other metals so that they are of major importance for the mining industry. In order to obtain gold from ore, solutions of cyanides are most effective. However, despite the fact that they are highly toxic for humans and wildlife, large quantities from mining processes often end up in the environment. Cyanides in very low concentrations are ubiquitous in nature and nearly all organisms have enzymes to detoxify them. Fruits and seeds, especially pits of many plants, such as cherries, peaches, almonds and lima beans, contain cyanogens capable of releasing free cyanides following enzymatic degradation [1]. The edible portion (the roots) of the cassava plant (a food staple in many parts of the world) is also cyanogenic [2].

Cyanides have been used throughout history as a poison. The Roman emperor Nero used cherry laurel water to poison members of his family and others who displeased him. Napoleon III proposed the use of cyanides on soldier's bayonets to enhance effectiveness [3]. Cyanides were used as a chemical weapon in their hydrogenated gaseous form HCN since World War I [4,5]. Cyanides were also called "blood agents", which is an antiquated military term. At the time of the introduction of cyanides in World War I, the other deployed chemical agents caused mainly local effects: riot control agents injured the skin and mucous membranes after direct contact, whereas Phosgene damaged the lungs after inhalation. In contrast, cyanides led to systemic effects after inhalation and were thought to be carried in the blood [3]. Other supposed military uses of cyanides include Japanese attacks on China before and during World War II. During World War II, the Germans used Zyklon B, a cyanides based rodenticide, to kill millions of people [3]. More recently, Iraq used cyanides against the Kurds in the 1980s [3]. However, recent environmental disasters and human tragedies caused by industrial accidents are due to cyanides. In 2000, a retaining wall failed at the Aurul gold processing plant in Romania, releasing a wave of cyanides and heavy metals that quickly propagated waterborne through Romania, Hungary, Serbia and Bulgaria, killing fish and other wildlife and poisoning drinking-water supplies [6].

On the other hand, these compounds have a broad variety of useful technical applications. Cyanides mostly appear as intermediates in the production of numerous downstream chemicals and are employed as solvents. A few examples are discussed below.

Backed by the chemical industry, substantial efforts were made in recent years by the molecular simulation community to tackle thermophysical properties of technically relevant fluid systems. This is particularly rewarding for substances which have hazardous properties, like being toxic or explosive, that render experimental studies difficult. Here, the results from a co-operation between academia and Lonza AG, Switzerland are presented. In this work, the fluid phase behavior of mixtures containing Cyanogen, Cyanogen chloride, Hydrogen cyanide and Acetonitrile were studied. For two pure compounds (Cyanogen and Cyanogen chloride), molecular force field models were developed here on the basis of quantum chemical (QC) calculations and optimizations to experimental vapor pressure and saturated liquid density data. Molecular models from prior works of our group were taken for the other compounds. Based on these molecular models, VLE data were predicted for three binary systems containing Cyanogen chloride, Cyanogen and Hydrogen cyanide. Furthermore, VLE of 11 binary mixtures containing Acetonitrile were simulated. These are Acetonitrile + (Acetone, Ammonia, Benzene, Chlorobenzene, Chloroform, Cyanogen, Cyanogen chloride, Ethanol, Hydrogen cyanide, Methanol, Toluene).

2 Molecular model class

The present molecular models include three groups of potential parameters. These are the geometric parameters, specifying the positions of different interaction sites, the electrostatic parameters, defining the polar interactions in terms of point charges, dipoles or quadrupoles, and the dispersive and repulsive parameters, determining the attraction by London forces and the repulsion by electronic orbital overlaps. Here, the Lennard-Jones (LJ) 12-6 potential [7,8] was used to describe the dispersive and repulsive interactions. The total intermolecular interaction

3

energy thus writes as

$$
\begin{aligned}
U = \sum_{i=1}^{N-1} \sum_{j=i+1}^{N} \Bigg\{ & \sum_{a=1}^{S_i^{\text{LJ}}} \sum_{b=1}^{S_j^{\text{LJ}}} 4\varepsilon_{ijab} \left[\left(\frac{\sigma_{ijab}}{r_{ijab}} \right)^{12} - \left(\frac{\sigma_{ijab}}{r_{ijab}} \right)^{6} \right] + \\
& \sum_{c=1}^{S_i^{\text{e}}} \sum_{d=1}^{S_j^{\text{e}}} \frac{1}{4\pi\epsilon_0} \Bigg[\frac{q_{ic}q_{jd}}{r_{ijcd}} + \frac{q_{ic}\mu_{jd} + \mu_{ic}q_{jd}}{r_{ijcd}^2} \cdot f_1(\boldsymbol{\omega}_i, \boldsymbol{\omega}_j) + \frac{q_{ic}Q_{jd} + Q_{ic}q_{jd}}{r_{ijcd}^3} \cdot f_2(\boldsymbol{\omega}_i, \boldsymbol{\omega}_j) + \\
& \frac{\mu_{ic}\mu_{jd}}{r_{ijcd}^3} \cdot f_3(\boldsymbol{\omega}_i, \boldsymbol{\omega}_j) + \frac{\mu_{ic}Q_{jd} + Q_{ic}\mu_{jd}}{r_{ijcd}^4} \cdot f_4(\boldsymbol{\omega}_i, \boldsymbol{\omega}_j) + \frac{Q_{ic}Q_{jd}}{r_{ijcd}^5} \cdot f_5(\boldsymbol{\omega}_i, \boldsymbol{\omega}_j) \Bigg] \Bigg\}, \quad (1)
\end{aligned}
$$

where r_{ijab}, ε_{ijab}, σ_{ijab} are the distance, the LJ energy parameter and the LJ size parameter, respectively, for the pair-wise interaction between LJ site a on molecule i and LJ site b on molecule j. The permittivity of the vacuum is ϵ_0, whereas q_{ic}, μ_{ic} and Q_{ic} denote the point charge magnitude, the dipole moment and the quadrupole moment of the electrostatic interaction site c on molecule i and so forth. The expressions $f_x(\boldsymbol{\omega}_i, \boldsymbol{\omega}_j)$ stand for the dependence of the electrostatic interactions on the orientations $\boldsymbol{\omega}_i$ and $\boldsymbol{\omega}_j$ of the molecules i and j [9,10]. Finally, the summation limits N, S_x^{LJ} and S_x^{e} denote the number of molecules, the number of LJ sites and the number of electrostatic sites, respectively.

It should be noted that a point dipole may, e.g. when a simulation program does not support this interaction site type, be approximated by two point charges $\pm q$ separated by a distance l. Limited to small l, this distance may be chosen freely as long as $\mu = ql$ holds. Analogously, a linear point quadrupole can be approximated by three collinear point charges q, $-2q$ and q separated by l each, where $Q = 2ql^2$ [11].

For a given molecule, i.e. for a pure fluid throughout, the interactions between LJ sites of different type were defined here by applying the standard Lorentz-Berthelot combining rules [12,13]

$$
\sigma_{ijab} = \frac{\sigma_{iiaa} + \sigma_{jjbb}}{2}, \quad (2)
$$

and

$$
\varepsilon_{ijab} = \sqrt{\varepsilon_{iiaa}\varepsilon_{jjbb}}. \quad (3)
$$

4

3 Molecular pure substance models

All molecules studied in the present work do not exhibit significant conformational changes. Hence their internal degrees of freedom were neglected and the molecular models were chosen to be rigid. In a first step, the geometric data of the molecules, i.e. bond lengths, angles and dihedrals, were determined by QC calculations. Therefore, a geometry optimization was carried out via an energy minimization using the GAMESS(US) package [14]. The Hartree-Fock level of theory was applied with a relatively small (6-31G) basis set. Intermolecular electrostatic interactions mainly occur due to the static polarity of single molecules that can well be obtained by QC. Here, the Møller-Plesset 2 level of theory was used that considers electron correlation in combination with the polarizable 6-31G basis set. The resulting electron distribution was approximated by dipoles or quadrupoles. The atomic charges were estimated here by the Mulliken method [15].

3.1 Cyanogen

Cyanogen plays an important role in many organic reactions and it can be used as a high-energy fuel in the chemical industry or as a missile propellant [16]. Cyanogen is used in organic syntheses [16], as a pesticide [16], fumigant [16] or in gold extraction processes [17]. It should be noted that Gay-Lussac was first person who synthesized Cyanogen in 1815 [16] and gave it its name.

A new molecular model was developed in this work for Cyanogen ($N \equiv C - C \equiv N$) based on QC information on molecular geometry and electrostatics. This Cyanogen model consists of four LJ sites, i.e. one for every atom. The polarity was modeled by a one relatively strong point quadrupole (-9.91 DÅ) located in the center of mass. Magnitude and orientation of the quadrupole, being along the molecular axis, were passed on from the QC calculations. All geometric data of the molecular model were determined by QC calculations.

The four parameters of the LJ sites, i.e. σ_N, ε_N, σ_C and ε_C, were adjusted to experimental VLE data. All parameters of the molecular model are given in Table 1. Table 2 presents the critical properties of Cyanogen predicted on the basis of the present molecular model. The critical prop-

erties were determined through fits to the present VLE simulation results as suggested by Lotfi et al. [18]. The pure substance VLE simulation results for Cyanogen are shown in Figures 1 to 3, where they are compared to experimental data and the DIPPR correlations [19]. No other molecular models for Cyanogen were found in the literature.

Only few experimental data for the saturated liquid density of Cyanogen are available [20–22]. The majority of the data cover the temperature range from 240 to 290 K only. A good agreement between simulation and experiment was achieved: the estimated deviation of saturated liquid density in this temperature range is 0.6 %, cf. Figure 4. A large number of experimental data points for the vapor pressure of Cyanogen are available in the literature [21,23–28]. Despite the good experimental data base, the desired quality was not achieved by the present optimization without significantly altering the quadruple magnitude. The model yields an average deviation in vapor pressure of 13 % over the full temperature range.

3.2 Cyanogen chloride

Cyanogen chloride is a toxic gas which was historically deployed in chemical warfare. It continues to be produced in limited amounts for industrial applications. Currently, it is used in fumigants [16], metal cleaners [16,29], the production of synthetic rubber [16] or in chemical synthesis [16].

Cyanogen chloride ($N \equiv C - Cl$) was modeled in the present work with three LJ sites, i.e. one for every atom. The electrostatic interactions were described by one dipole and one quadrupole that are both oriented along the molecular axis. All geometric data of the molecular model, i.e. bond lengths and angles, were determined by QC calculations in the same way as for Cyanogen. The six parameters of the LJ sites, i.e. σ_N, ε_N, σ_C, ε_C, σ_{Cl} and ε_{Cl}, were adjusted to experimental VLE data. The optimized parameter set of the new molecular model is presented in Table 1, its critical properties are compared to reference data in Table 2. No other molecular models were found in the literature for Cyanogen chloride.

The pure substance VLE simulation results are shown in Figures 1 to 3, where they are compared to experimental data and the DIPPR correlations [19]. Some experimental data sets for Cyanogen

chloride are available for comparison [20,22,30–36]. However, the majority of these data cover the temperature range from 260 to 290 K only. A very good agreement was obtained with the present model in this temperature range, yielding mean unsigned errors in saturated liquid density, vapor pressure and enthalpy of vaporization of 0.3, 2.1 and 3.3 %, respectively, cf. Figure 4.

For pure Cyanogen chloride, predicted data on the second virial coefficient and the isobaric heat capacity are available from DIPPR. Figures 5 and 6 show the simulation results compared to correlations of predicted data taken from DIPPR [19]. The present second virial coefficient agrees well with the DIPPR correlation at high temperatures, however below 300 K, the two predictive models disagree. The isobaric heat capacity c_p was determined here by molecular simulation and compared to predicted data from Chueh et al. [32]. Over the entire temperature range, the c_p data from simulation are consistently higher, cf. Figure 6. The deviations are between 9 and 14 %. Note that the residual isobaric heat capacity was determined by simulation. For the comparison in Figure 6, the ideal gas contribution to the heat capacity was taken from DIPPR [37,38] and added to the simulation results.

3.3   Hydrogen cyanide

Hydrogen cyanide is an important industrial chemical of which over a million tonnes are produced globally each year. It is synthesized by a reaction of Methane and Ammonia in air at high temperature. In Water, Hydrogen cyanide acts as a weak acid, donating its proton to Water. The remaining cyanide anion (CN^-) may react by donating an electron pair to Carbon with partial positive charge character in an organic compound. Consequently, Hydrogen cyanide can be used to yield nitrile compounds, which contain a Nitrogen atom that is triple-bonded to a Carbon atom on a carbon chain. This property makes Hydrogen cyanide useful in the synthesis of organic compounds like pharmaceuticals [29] or chelating agents [29].

The molecular model for Hydrogen cyanide ($N\equiv C-H$) was taken from Eckl et al. [39], because no other molecular models were found in the literature. It consists of two LJ sites, one for the methine group and one for the nitrogen atom, one dipole and one quadrupole that are both

oriented along the molecular axis. The model by Eckl et al. shows mean unsigned deviations to experimental data of 1.0 % for the saturated liquid density, 7.2 % for the vapor pressure and 12.2% for the enthalpy of vaporization over the whole temperature range from the triple point to the critical point.

3.4 Acetonitrile

Acetonitrile is a core solvent in the chemical industry, particularly for the pharmaceutical sector, which accounts for over 70 % of the total market. The popularity of Acetonitrile is due to its excellent solvation ability with respect to a wide range of polar and non-polar solutes as well as other favorable properties, such as low freezing/boiling points, low viscosity and relatively low toxicity. Acetonitrile is often used in GC analysis, UV analysis, TLC and HPLC applications as well as other wet chemistry test methods [40]. Acetonitrile, also called Methyl cyanide, is the simplest organic nitrile. Its reaction with Cyanogen chloride at temperatures above 600 ^{0}C supplies Malononitrile, which is an important building block for the syntheses of pharmaceuticals (e.g. Triamterene, Adenine or Methotrexate), Thiamin (vitamin B1), pesticides or dyestuffs for photography [40].

Several molecular models for Acetonitrile ($N\equiv C-CH_3$) are available in the literature: Eckl et al. [39], Jorgensen and Briggs [41], Price et al. [42], Guárdia et al. [43], Nikitin and Lyubartsev [44], Hloucha and Deiters [45], Wick et al. [46] and Deublein et al. [47]. The molecular model for Acetonitrile by Deublein et al. [47], that is based on the LJ approach with one superimposed dipole, was used here. The geometry of this molecular model and its electrostatics were specified according to QC data, while several LJ parameters were adjusted to experimental VLE data with an automated optimization procedure. This molecular model reproduces the experimental reference data with average deviations of 0.1 %, 4.7 % and 3.9 % for saturated liquid density, vapor pressure and enthalpy of vaporization for temperatures between 60 and 99 % of its critical temperature.

3.5 Molecular models for the other compounds

The present work is devoted to the development and assessment of molecular models for cyanides and their mixtures. Apart from the VLE data for the pure cyanides and the binary mixtures Cyanogen chloride + Hydrogen cyanide and Hydrogen cyanide + Acetonitrile, experimental data are primarily available in the literature for binary mixtures containing Acetonitrile. Binary Acetonitrile mixtures with the following components were thus also simulated in the present work: Acetone, Ammonia, Benzene, Chlorobenzene, Chloroform, Ethanol, Methanol and Toluene. The employed molecular models were taken from preceding publications of our group and are briefly described in the following.

The molecular model for Ammonia was taken from Eckl et al. [48]. It consists of a single LJ site for the dispersive and repulsive interactions. The electrostatic interactions as well as hydrogen bonding were modeled by four superimposed partial charges. The new molecular model of Acetone by Windmann and Vrabec [49] was chosen here to calculate the VLE of Acetonitrile + Acetone. It is based on four LJ sites plus one relatively strong dipole (3.44 D) and one relatively weak quadrupole (0.73 DÅ). In comparison with alternative Acetone models from the literature [50,51], this model better represents the VLE properties in the relevant temperature range. The molecular models that were used for Benzene, Chlorobenzene and Toluol were discussed in detail by Huang et al. [52]. The molecular model for Chloroform was taken from Stoll et al. [53] and is of two-center LJ plus point dipole type. The molecular models for Methanol and Ethanol were developed by Schnabel et al. [54,55] and consist of two (Methanol) or three (Ethanol) LJ sites and three point charges each.

4   Molecular mixture models

On the basis of defined pairwise additive pure fluid models, molecular modeling of mixtures reduces to modeling the interactions between unlike molecules. Unlike interactions are of two different types here. The unlike electrostatic interactions, e.g. between dipoles or quadrupoles, were treated in a physically straightforward way, simply using the laws of electrostatics.

Unfortunately, the unlike dispersive attraction is not straightforward. If a mixture A + B is modeled on the basis of Lennard-Jones potentials, the knowledge of the unlike LJ parameters σ_{ijab} and ε_{ijab} for the pair-wise interaction between LJ site a on molecule i of component A and LJ site b on molecule j of component B is required. Due to the fact that there is no sound physical framework for their determination, the broadly employed Lorentz-Berthelot combining rules are the usual starting point [56]. Applying σ_{ijab} and ε_{ijab} as given by equations (2) and (3) allows for the prediction of mixture properties from pure fluid data alone [56–60]. However, as shown in these publications, a significant improvement can be achieved by introducing one state independent binary interaction parameter ξ to adjust the unlike energy parameter

$$\varepsilon_{ijab} = \xi\sqrt{\varepsilon_{iiaa}\varepsilon_{jjbb}}. \tag{4}$$

It allows to fine-tune the unlike dispersive attraction, a property which is very challenging even for current QC approaches [61]. It should be pointed out that A and B are molecule species that may each be described by several LJ sites with different energy parameters ϵ. Thus, ξ is a single overall parameter that acts consistently on all individual unlike LJ interactions of the molecule pair A + B.

For VLE, it was shown in [56] that ξ can be adjusted to a single experimental binary vapor pressure. Specifying temperature and saturated liquid composition, ξ has hardly any influence on the saturated liquid density and a minor influence on the saturated vapor composition. The benefit of ξ lies in a significantly enhanced representation of the two-phase envelope. The binary interaction parameter was adjusted here following the same procedure as in [57–60,62].

5 Peng-Robinson equation of state

Cubic equations of state (EOS) are standard tool to correlate experimental data and are therefore a workhorse for many technical applications. In the present work, the Peng-Robinson EOS with the quadratic Van der Waals one-fluid mixing rule was used to adjust binary experimental data.

The Peng-Robinson EOS [63] is given by

$$p = \frac{RT}{v - b} - \frac{a}{v(v + b) + b(v - b)}, \tag{5}$$

where the temperature dependent parameter a is defined by

$$a = \left(0.45724 \, \frac{R^2 T_c^{\,2}}{p_c}\right) \left[1 + \left(0.37464 + 1.54226 \, \omega - 0.26992 \, \omega^2\right) \left(1 - \sqrt{\frac{T}{T_c}}\right)\right]^2. \tag{6}$$

The constant parameter b is

$$b = 0.07780 \, \frac{RT_c}{p_c}. \tag{7}$$

Therein, critical temperature T_c, critical pressure p_c, acentric factor ω and the molar mass M of the pure substance are needed, cf. Table 3.

To apply the Peng-Robinson EOS to mixtures, mixed parameters a_m and b_m have to be defined. For this purpose, a variety of mixing rules can be found in the literature. Here, the quadratic Van der Waals one-fluid mixing rule [63] was chosen. It states that the pure substance parameters a and b have to be replaced by

$$a_m = \sum_i \sum_j x_i x_j a_{ij}. \tag{8}$$

The indices i and j denote the components, with

$$a_{ij} = \sqrt{a_i a_j}(1 - k_{ij}), \tag{9}$$

where k_{ij} is an adjustable binary parameter to correlate experimental data. The constant parameter of the mixture is defined as

$$b_m = \sum_i x_i b_i. \tag{10}$$

The results of the Peng-Robinson EOS are presented below and validated by comparison to data from experiment and simulation.

6 Binary vapor-liquid equilibria

Based on the discussed molecular models, VLE data were predicted for binary systems containing Cyanogen, Cyanogen chloride, Hydrogen cyanide and Acetonitrile. For two of the six binary systems that can be formed from these compounds, i.e. Cyanogen chloride + Hydrogen cyanide and Hydrogen cyanide + Acetonitrile experimental data were available. The experimental vapor pressure at one liquid mole fraction was taken to adjust the binary parameter of the molecular model. It should be pointed out that the saturated vapor composition was not included in the adjustment so that the simulation data along the saturated vapor line are fully predictive and thus can well be used to assess the mixture models. For the remaining four binary mixtures, no experimental VLE data were available. Therefore the VLE were predicted for these systems by molecular simulation and the results were compared with the Peng-Robinson EOS. Moreover, VLE data were predicted for eight binary mixtures containing Acetonitrile, where the choice was driven by the availability of experimental VLE data and molecular models.

For orientation and comparison, the results of the Peng-Robinson EOS [64] with adjusted binary parameter k_{ij} of the quadratic mixing rule are also presented. The EOS was optimized to the same state point as the molecular model. The adjusted binary parameter k_{ij} is given in Table 4.

6.1 Cyanogen chloride + Hydrogen cyanide

Cyanogen chloride and Hydrogen cyanide are similar in their toxicity so that experiments are often avoided. For these systems, experimental data are available only from a single source from 1946 [65]. Gordon et al. [65] have investigated the binary VLE for the system Cyanogen chloride + Hydrogen cyanide at 288.15 K. The compositions of the coexisting phases under VLE were determined by slow isothermal distillation and the vapor pressure by a mercury manometer [65]. The present simulations were also carried out at constant temperature of 288.15 K. The experimental vapor pressure at a liquid mole fraction of $x_{NCCl} = 0.5$ mol/mol was taken to adjust the binary parameter of the molecular model ($\xi = 1.023$) and of the Peng-Robinson EOS ($k_{ij} = 0.03$). Figure 7 shows the VLE of Cyanogen chloride + Hydrogen cyanide at 288.15 K from

experiment, simulation and the Peng-Robinson EOS. It can be seen that the results obtained by molecular simulation agree well with the experimental results and the Peng-Robinson EOS.

6.2   Hydrogen cyanide + Acetonitrile

Figure 8 shows the isobaric VLE of Hydrogen cyanide + Acetonitrile at 0.1013 MPa from the experiments by Jiang et al. [66], present simulations and the Peng-Robinson EOS. The binary parameters $\xi = 1.02$ and k_{ij} = -0.0365 were adjusted to the vapor pressure measured by Jiang et al. [66] at 319.25 K and a liquid mole fraction of x_{HCN} = 0.5174 mol/mol. It can be seen in Figure 8 that the predictions obtained by molecular simulation with the binary interaction parameter $\xi = 1.02$ and those from the Peng-Robinson EOS with k_{ij} = -0.0365 agree well with the experimental data.

6.3   Cyanogen + Cyanogen chloride

The mixture Cyanogen chloride + Cyanogen is one of the four cases in this study for which no experimental VLE data were available. Without experimental data for adjustment, $\xi = 1$ was adopted for the molecular mixture model. Simulation data on the saturated liquid line at x_{NCCN} = 0.4 mol/mol were taken to adjust the binary parameter of the Peng-Robinson EOS (k_{ij} = -0.025). Figure 9 depicts the VLE of Cyanogen chloride + Cyanogen at 313.15 K. It can be seen in Figure 9 that the results obtained by molecular simulation agree well with the Peng-Robinson EOS outside of the Cyanogen-rich region. Considering the slightly too low vapor pressure of the Cyanogen pure substance model at this temperature, cf. Figure 4, it can be seen that the slope of the saturated liquid line of the mixture is followed reasonably well.

6.4   Cyanogen chloride + Acetonitrile

As for the previous mixture, no experimental VLE data for Cyanogen chloride + Acetonitrile were available. Without experimental data for adjustment, $\xi = 1$ was adopted for the molecular model. The VLE results of Cyanogen chloride + Acetonitrile are presented in Figure 10 at 313.15 K. The vapor pressure at a liquid mole fraction of x_{NCCl} = 0.5 mol/mol was taken to adjust the

binary parameter of the Peng-Robinson EOS k_{ij} = -0.01. It can be seen in Figure 10 that the predictions at 313.15 K obtained by molecular simulation and those from the Peng-Robinson EOS are in very good agreement, some deviations are present on the saturated vapor line.

6.5   Cyanogen + Acetonitrile

Based on the two pure substance models described above, the VLE of the binary mixture Cyanogen + Acetonitrile was simulated. Binary VLE data were generated on the basis of pure substance properties only, because no experimental data for this mixture were available in the literature. The results of the Peng-Robinson EOS with adjusted binary parameter k_{ij} of the quadratic mixing rule are also shown. Figure 11 shows the VLE of Cyanogen + Acetonitrile at 333.15 K from molecular simulation and the Peng-Robinson EOS. Without any experimental data for adjustment, the vapor pressure predicted by the molecular model ($\xi = 1$) at a liquid mole fraction of x_{NCCN} = 0.5 mol/mol was taken to adjust the binary parameter of the Peng-Robinson EOS (k_{ij} = -0.225). The simulation results are in very good agreement with the Peng-Robinson EOS over the full composition range.

6.6   Cyanogen + Hydrogen cyanide

Isothermal VLE data of Cyanogen + Hydrogen cyanide are presented in Figure 12 at 313.15 K. No experimental data were available so that the simulation data can only be compared to the Peng-Robinson EOS. Without any experimental data for adjustment, the simulation results for the binary interaction parameter of the molecular model with $\xi = 1$ were taken to adjust the corresponding binary parameter of the Peng-Robinson EOS (k_{ij} = -0.125). In analogy to the mixture Cyanogen + Cyanogen chloride at 313.15 K, the results obtained by molecular simulation agree well with the Peng-Robinson EOS outside of the Cyanogen-rich region. This is again caused by a too low vapor pressure of the Cyanogen pure substance model at low temperatures, cf. Figure 4.

6.7 Binary mixtures with Acetonitrile

Many technical processes in chemical engineering are dealing with fluid mixtures containing Acetonitrile. In this work, a total of eight binary mixtures containing Acetonitrile were simulated. These are Acetonitrile + (Acetone, Ammonia, Benzene, Chlorobenzene, Chloroform, Ethanol, Methanol, Toluene). Depending on the available experimental data, the simulation results for binary mixtures are presented here in pressure or temperature vs. mole fraction phase diagrams. For all studied mixtures, experimental VLE data were available for adjustment and comparison. Throughout, the Peng-Robinson EOS was adjusted to the same experimental data point as the binary interaction parameter ξ.

Figure 13 shows the VLE simulation results for Ammonia + Acetonitrile at 0.59 MPa in comparison to experimental VLE data provided by Tyvina and Fokina [67] and the Peng-Robinson EOS. The binary parameters $\xi = 0.97$ and $k_{ij} = $ -0.015 were adjusted to the experimental vapor pressure at 313.15 K for a liquid mole fraction of $x_{NH3} = 0.42$ mol/mol. It can be seen in Figure 13 that the results obtained by molecular simulation agree well with the experimental data on the saturated liquid line, but overestimate the Ammonia content on the saturated vapor line. In the Acetonitrile-rich region, the narrow two-phase envelope is well predicted by simulation, whereas in the Ammonia-rich region, the experimental data yield a qualitatively different form. The Peng-Robinson EOS yields the same course of the saturated vapor line as the molecular model.

The binary VLE of Chloroform + Acetonitrile is presented in Figure 14 for the temperature 303.15 K. The experimental vapor pressure by Lazarte et al. [68] at the same temperature and $x_{CHCl3} = 0.56$ mol/mol was taken to adjust the binary parameter of the molecular model ($\xi = 0.99$) and of the Peng-Robinson EOS ($k_{ij} = 0.021$). Despite the significant deviations between calculated, simulated and measured vapor pressures for the pure compounds (especially for acetonitrile), the agreement in phase envelope is satisfactory.

Figure 15 shows the isothermal VLE simulation results for Acetonitrile + Chlorobenzene at 328.15 K in comparison to experimental data provided by Nagata [69] and the Peng-Robinson

EOS. The binary parameters $\xi = 0.96$ and $k_{ij} = 0.084$ were adjusted to the experimental vapor pressure at 328.15 K at a liquid mole fraction of $x_{\text{C2H3N}} = 0.488$ mol/mol. It can be seen in Figure 15 that the results obtained by molecular simulation agree well with the experimental results on the saturated liquid line, but overestimate the Acetonitrile content on the saturated vapor line.

Figure 16 shows the isothermal VLE simulation results of Acetone + Acetonitrile at 318.15 K from experiment, simulation and Peng-Robinson EOS. For this mixture, it can be seen that the very narrow shape of the two-phase envelope was predicted correctly. The experimental vapor pressure by Brown and Smith [70] at 318.15 K and $x_{\text{C3H6O}} = 0.481$ mol/mol was taken to adjust the binary parameter of the molecular model ($\xi = 1.0$) and of the Peng-Robinson EOS ($k_{ij} = 0.017$). It should be noted that the description of the interactions between LJ sites of unlike molecules was in this case the same as the standard Lorentz-Berthelot combining rule. For $\xi = 1$, the results obtained with molecular simulation are also close to those from the Peng-Robinson EOS on the saturated liquid line, however, the simulated vapor pressure for Acetonitrile shows significant deviations. For the mixture Acetone + Acetonitrile, isobaric experimental VLE data at ambient pressure were available as well. Figure 17 shows the isobaric VLE of Acetone + Acetonitrile at 0.10133 MPa from the experiments carried out by Gorshkov et al. [71] and Pratt [72], present simulations and the Peng-Robinson EOS. The adjusted binary parameters were the same as for the isothermal VLE ($\xi = 1$ and $k_{ij} = 0.017$). It can be seen that the simulation results match almost perfectly with the experimental data on the saturated liquid line. On the saturated vapor line, the experimental data and the simulation results exhibit some scatter, but the agreement is reasonable.

In Figures 18 to 21, the VLE of Acetonitrile + Ethanol and Methanol + Acetonitrile are presented. For both mixtures, isothermal and isobaric VLE experimental data are available [73–76]. To adjust the binary parameter of the models, isothermal experimental vapor pressure data at equimolar composition by Sugi and Katayama [73] for Acetonitrile + Ethanol and by Dohnal et al. [75] for Methanol + Acetonitrile were taken. The adjusted binary parameters ξ and k_{ij} are given in Table 4. It should be noted that the parameter for the interactions between LJ sites of

unlike molecules was in this case unusually low, i.e. $\xi < 0.9$. The binary systems Acetonitrile + Ethanol and Methanol + Acetonitrile have an azeotrope. The location of the azeotrope from present simulations is in good agreement with that from the literature [73–76]. For these mixtures, experimental data and simulation results agree very well on the saturated liquid line as well as on the saturated vapor line.

The VLE of the binary system Benzene + Acetonitrile is shown in Figures 22 and 23. Present simulation results are compared to experimental data by Monfort [77] and Di Cave and Mazzarotta [78] as well as to the Peng-Robinson EOS [64] for the temperature 343.15 K as well as for the pressure 0.1013 MPa. The experimental vapor pressure by Monfort [77] at 343.15 K and $x_{C6H6} = 0.504$ mol/mol was taken to adjust the binary parameter of the molecular model ($\xi = 1.024$) and of the Peng-Robinson EOS ($k_{ij} = 0.075$). This mixture is azeotropic too, the azeotropic composition at 343.15 K is $x_{C6H6} \approx 0.53$ mol/mol. The azeotrope can also be seen in the isobaric VLE, where it is also approximately at equimolar composition. Both the simulation results and the Peng-Robinson EOS match well with the experimental data, but the phase envelope from simulation is a little wider than the one from experiment. However, the simulated vapor pressure of both pure compounds is lower than the experiment.

In Figures 24 and 25, VLE data of Acetonitrile + Toluene are presented. Figure 24 shows the simulation results at 343.15 K in comparison to experimental VLE data provided by Monfort [77] and the Peng-Robinson EOS. The experimental vapor pressure at 343.15 K and $x_{C2H3N} = 0.52$ mol/mol was taken to adjust the binary parameter of the molecular model ($\xi = 0.918$) and of the Peng-Robinson EOS ($k_{ij} = 0.081$). Like the preceding two systems, this mixture is azeotropic and has a temperature minimum. In this case, the azeotropic point lies at $x_{C2H3N} \approx 0.86$ mol/mol. It can be seen in Figure 24 that the experimental data and the simulation results exhibit some scatter, but the topology is satisfactory. The vapor pressures of pure compounds was underestimated. Figure 25 shows the isobaric VLE simulation results with $\xi = 0.918$ for Acetonitrile + Toluene at 0.028 MPa in comparison to experimental VLE data provided by Di Cave and Mazzarotta [78] and the Peng-Robinson EOS with $k_{ij} = 0.081$. Figure 25 shows that the narrow two-phase envelope in the Acetonitrile-rich region was well predicted by simulation,

whereas in the Toluene-rich region, the experimental data exhibit a qualitatively different form.

7 Conclusion

Molecular modeling and simulation was applied to predict the phase behavior of pure fluids and binary mixtures containing cyanides. New molecular models, based on quantum chemical information on molecular geometry and electrostatics, were developed for Cyanogen and Cyanogen chloride. Furthermore, experimental data on the saturated liquid density and the vapor pressure were taken into account to optimize the LJ parameters of these pure substance models. These pure fluid properties were represented accurately from the triple point to the critical point. It was also shown that both models are capable to reasonably predict the second virial coefficient. Unfortunately, few experimental data on VLE properties of binary mixtures containing these compounds were available.

For an optimized description of the binary VLE, the unlike dispersive interaction was adjusted for ten of the 14 studied binary systems to a single experimental vapor pressure. With these binary mixture models, VLE data were predicted for a wide range of compositions. For four binary mixtures (i.e. all mixtures with Cyanogen as well as Cyanogen chloride + Acetonitrile), no experimental VLE data were available. For these mixtures, VLE were predicted with $\xi = 1$ for the molecular model. Furthermore, the Peng-Robinson EOS with the quadratic mixing rule was adjusted for all studied binary mixtures to experimental data or, if not available, to the present simulation data. Generally, the predictions show a good agreement with the experimental VLE data and the Peng-Robinson EOS.

This work shows that molecular modeling and simulation can successfully be used to predict thermophyiscal data of industrially important pure fluids and mixtures that have a hazardous nature.

putational Molecular Engineering (BZS). The simulations were carried out on the national super computer NEC Nehalem Cluster at the High Performance Computing Center Stuttgart (HLRS) and on the HP X6000 super computer at the Steinbuch Centre for Computing, Karlsruhe. The authors are grateful for financial support of this work by Lonza AG. Fruitful discussions and suggestions from colleagues of this company are highly appreciated. Furthermore, we would like to thank Patrick Biemelt, Tatjana Janzen and Yujia Zhai for carrying out the part of simulation work.

8 Appendix: Simulation details

The Grand Equilibrium method [79] was used to calculate VLE data for all systems and the calculations were performed with the $ms2$ simulation code [80]. For the liquid, Monte-Carlo simulations were performed in the isobaric-isothermal (NpT) ensemble. There, the number of molecules was 864 for pure fluids and for mixtures. The gradual insertion method [81,82] was used to calculate the chemical potential for all binary systems. Starting from a face centered cubic lattice, 30 000 Monte Carlo cycles with the first 10 000 cycles in the canonical (NVT) ensemble were carried out for equilibration and 100 000 for production. Each cycle contained a number of attempts to displace and rotate molecules equal to the actual number of molecules N plus one volume move. Every cycle, $10 \times N$ fluctuating state change moves, $10 \times N$ fluctuating particle translation/rotation moves, and $50 \times N$ biased particle translation/rotation moves were sampled to determine the chemical potential. For the corresponding vapor, Monte Carlo simulations in the pseudo-μVT ensemble were carried out. The simulation volume was adjusted to lead to an average number of 500 molecules in the vapor phase. After 10 000 initial NVT Monte Carlo cycles, starting from a face centered cubic lattice, 25 000 equilibration cycles in the pseudo-μVT ensemble were sampled. The length of the production run was 100 000 cycles. The cut-off radius was set to 15 Å throughout and a center of mass cut-off scheme was employed. LJ long-range interactions beyond the cut-off radius were corrected employing angle averaging as proposed by Lustig [83]. Electrostatic interactions were calculated using the reaction field method [9]. Statistical uncertainties of the simulated values were estimated by a block averaging method

[84].

References

[1] F. Dicenta, V. Berenguer, N. Grane, M.L. Martín, A. León, P. Martinez-Gomez, J. Agric. Food Chem. 50 (2002) 2149-2152.

[2] D.D. Ngudi, Y.H. Kuo, F. Lambein, Food Chem. Toxicol. 41 (2003) 1193-1197.

[3] C.P. Holstege, T. Neer, G.B. Saathoff, R.B. Furbe, Criminal Poisoning: Clinical and Forensic Perspectives, Jones and Bartlett Publishers, Sudbury, 2011.

[4] R.A. Greenfield, B.R. Brown, J.B.Hutchins, Am. J. ed. Sci. 323 (2002) 326-340.

[5] M. Rosenbloom, J.B. Leikin, S.N. Vogel, Am. J. Ther. 9 (2002) 5-14.

[6] S.A. Cunningham, Disasters 29 (2005) 99-128.

[7] J.E. Jones, Proc. Roy. Soc. 106A (1924) 441-462.

[8] J.E. Jones, Proc. Roy. Soc. 106A (1924) 463-477.

[9] M.P. Allen, D.J. Tildesley, Computer simulations of liquids, Oxford University Press, Oxford, 1987.

[10] C.G. Gray, K.E. Gubbins, Theory of molecular fluids. 1. Fundamentals, Clarendon Press, Oxford, 1984.

[11] C. Engin, J. Vrabec, H. Hasse, Mol. Phys. 109 (2011) 1975-1982.

[12] H.A. Lorentz, Ann. Phys. 12 (1881) 127-136.

[13] D. Berthelot, Compt. Rend. Ac. Sc. 126 (1898) 1703-1706.

[14] M.W. Schmidt, K.K. Baldridge, J.A. Boatz, S.T. Elbert, M.S. Gordon, J.H. Jensen, S. Koseki, N. Matsunaga, K.A. Nguyen, S. Shujun, T.L. Windus, M. Dupuis, A.M. Montgomery, J. Comput. Chem. 14 (1993) 1347-1363.

[15] R.S. Mulliken, J. Chem. Phys. 36 (1962) 3428-3440.

[16] P. Patnaik, Handbook of Inorganic Chemicals, McGraw-Hill, New York, 2003.

[17] A. Akcil, Biotech. Adv. 21 (2003) 501-511.

[18] A. Lotfi, J. Vrabec, J. Fischer, Mol. Phys. 76 (1992) 1319-1333.

[19] R.L. Rowley, W.V. Wilding, J.L. Oscarson, Y. Yang, N.A. Zundel, T.E. Daubert, R.P. Danner, DIPPR Information and Data Evaluation Manager for the Design Institute for Physical Properties, AIChE, New York, Version 5.0.2, 2011.

[20] R.P. Cook , P.L. Robinson, J. Chem. Soc. 19 (1935) 1001-1005.

[21] F. Ullmann, W. Gerhartz, Y.S. Yamamoto, Ullmann's Encyclopedia of Industrial Chemistry, fifth ed., VCH Publishers, Weinheim, 1985.

[22] R.C. Weast, Handbook of Chemistry and Physics, sixty-second ed., The Chemical Rubber Co., Cleveland, 1981.

[23] E.W. Washburn, International Critical Tables of Numerical Data, Physics, Chemistry, and Technology, McGraw-Hill, New York, 2003.

[24] R.A. Ruehrwein, W.F. Giauque, J. Am. Chem. Soc. 61 (1939) 2940-2944.

[25] J.H. Perry, D.C. Bardwell, J. Am. Chem. Soc. 47 (1925) 2629-2632.

[26] J.W. Terwen, Z. Phys. Chem. Leipzig 91 (1916) 469-499.

[27] J. Chappuis, C. Riviere, C. R. Hebd. Seanc. Acad. Sci. Paris 104 (1887) 1504-1505.

[28] M. Faraday, Philos. Trans. Roy. Soc. London 135 (1845) 155-177.

[29] HazDat database. Atlanta, GA, US Department of Health and Human Services, Public Health Service, Agency for Toxic Substances and Disease Registry, 2003. Available at http://www.atsdr.cdc.gov

[30] N.V. Steere, Handbook of Laboratory Safety, second ed., CRC Press, Boca Raton, 1971.

[31] N.I. Sax, Dangerous Properties of Industrial Materials, sixth ed., Van Nostrand Reinhold Co., New York, 1984.

[32] C.F. Chueh, A.C. Swanson, Chem. Eng. Prog. 51 (1973) 596-600.

[33] A.K. Macbeth, J.A. Mills, J. Chem. Soc. 67 (1945) 709-712.

[34] A. Klemenc, G. Wagner, Allgemein. Chem. 235 (1938) 427-430.

[35] D.E. Douglas, C.A. Winkler, Can. J. Res. 25 (1947) 381-386.

[36] M.K. Baranaev, V.V. Prokhorova, V.I. Suverova, Khim. Prom. 5 (1968) 390-390.

[37] D.P. Stevenson, J. Chem. Phys. 7 (1939) 171-174.

[38] B.J. McBride, S. Gordon, J. Chem. Phys. 35 (1961) 2198-2206.

[39] B. Eckl, J. Vrabec, H. Hasse, J. Phys. Chem. B. 112 (2008) 12710-12721.

[40] International Programme on Chemical Safety. World Health Organization. Accessed May 2010. Available at http://www.inchem.org/documents/ehc/ehc/ehc154.htm

[41] W.L. Jorgensen, J.M. Briggs, Mol. Phys. 63 (1988) 547-558.

[42] M.L.P. Price, D. Ostrovsky, W.L. Jorgensen, J. Comput. Chem. 22 (2001) 1340-1352.

[43] E. Guàrdia, R. Pinzoón, J. Casulleras, M. Orozco, F.J. Luque, Mol. Sim. 26 (2001) 287-306.

[44] A.M. Nikitin, A.P. Lyubartsev, J. Comput. Chem. 28 (2007) 2020-2026.

[45] M. Hloucha, U.K. Deiters, Mol. Phys. 90 (1997) 593-597.

[46] C.D. Wick, J.M. Stubbs, N. Rai, J.I. Siepmann, J. Phys. Chem. B 109 (2005) 18974-18982.

[47] S. Deublein, P. Metzler, J. Vrabec, H. Hasse, Mol. Sim. 39 (2012) 109-118.

[48] B. Eckl, J. Vrabec, H. Hasse, Mol. Phys. 106 (2008) 1039-1046.

[49] T. Windmann, J. Vrabec, (in preparation).

[50] J.M. Stubbs, J.J. Potoff, J.I. Siepmann, J. Phys. Chem. B 108 (2004) 17596-17605.

[51] N. Ferrando, V. Lachet, A. Boutin, J. Phys. Chem. B 114 (2010) 8680-8688.

[52] Y.-L. Huang, M. Heilig, H. Hasse, J. Vrabec, AIChE J. 52 (2011) 1043-1060.

[53] J. Stoll, J. Vrabec, H. Hasse, J. Chem. Phys. 119 (2003) 11396-11407.

[54] T. Schnabel, J. Vrabec, H. Hasse, Fluid Phase Equilib. 233 (2005) 134-143.

[55] T. Schnabel, A. Srivastava, J. Vrabec, H. Hasse, J. Phys. Chem. B 111 (2007) 9871-9878.

[56] T. Schnabel, J. Vrabec, H. Hasse, J. Mol. Liq. 135 (2007) 170-178.

[57] J. Stoll, Fortschritt-Berichte VDI, Reihe 3, Vol. 836, VDI-Verlag, Düsseldorf, 2005.

[58] J. Stoll, J. Vrabec, H. Hasse, AIChE J. 49 (2003) 2187-2198.

[59] J. Vrabec, J. Stoll, H. Hasse, Mol. Sim. 31 (2005) 215-221.

[60] J. Carrero-Mantilla, M. Llano-Restrepo, Mol. Sim. 29 (2003) 549-554.

[61] G. Guevara-Carrion, H. Hasse, J. Vrabec, Top. Curr. Chem. 307 (2012) 201-250.

[62] Y.-L. Huang, S. Miroshnichenko, H. Hasse, J. Vrabec, Int. J. Thermophys. 30 (2009) 1791-1810.

[63] J.M. Smith, H.C. Van Ness, M.M. Abbott, Introduction to chemical engineering thermodynamics, fifth ed., McGraw-Hill, New York, 1996.

[64] D.Y Peng, D.B. Robinson, Ind. Eng. Chem. Fundam. 15 (1976) 59-64.

[65] A.R. Gordon, G.C. Benson, Can. J. Res. B 24 (1946) 285-291.

[66] W. Jiang, Y. Zhang, M. Cao, S. Han, Zhejiang-Daxue-Xuebao 3 (1983) 25-41.

[67] T.N. Tyvina, V.V. Fokina, Fazovye ravnovesija i prakticheskie aspekty processov razdelenija produktov neftehimicheskogo sinteza, Sbornik nauchnyh trudov, Moskva, 1980.

[68] M. Lazarte, A.C. Gomez Marigliano, H.N. Solimo, J. Solution Chem. 33 (2004) 1549-1563.

[69] I. Nagata, J. Chem. Thermodyn. 16 (1984) 955-958.

[70] I. Brown, F. Smith, Aust. J. Chem. 13 (1960) 30-37.

[71] V.A. Gorshkov, S.Y. Pavlov, L.L. Karpacheva, G.A. Kirillova, Ispol'zovanie fiziko-himicheskih i matematicheskih metodov v issledovanii processov poluchenija monomerov i sinteticheskih kauchukov, Sbornik nauchnyh trudov, Moskva, 1979.

[72] H.R.C. Pratt, Trans. Inst. Chem. Engr. 25 (1947) 43-67.

[73] H. Sugi, T. Katayama, J. Chem. Eng. Japan 11 (1978) 167-172.

[74] V. Dohnal, F. Vesely, R. Holub, J. Pick, Collect. Czech. Chem. Commun. 47 (1982) 3177-3187.

[75] V. Dohnal, R. Holub, J. Pick, Collect. Czech. Chem. Commun. 42 (1977) 1445-1452.

[76] A. Tamir, J. Wisniak, J. Chem. Eng. Data 31 (1986) 363-364.

[77] J.-P. Monfort, J. Chem. Eng. Data 28 (1983) 24-27.

[78] S. Di Cave, B. Mazzarotta, J. Chem. Eng. Data 36 (1991) 293-297.

[79] J. Vrabec, H. Hasse, Mol. Phys. 100 (2002) 3375-3383.

[80] S. Deublein, B. Eckl, J. Stoll, S.V. Lishchuk, G. Guevara-Carrion, C.W. Glass, T. Merker, M. Bernreuther, H. Hasse, J. Vrabec, Comp. Phys. Commun. 182 (2011) 2350-2367.

[81] I. Nezbeda, J. Kolafa, Mol. Sim. 5 (1991) 391-403.

[82] J. Vrabec, M. Kettler, H. Hasse, Chem. Phys. Lett. 356 (2002) 431-436.

[83] R. Lustig, Mol. Phys. 65 (1988) 175-179.

[84] H. Flyvbjerg, H.G. Petersen, J. Chem. Phys. 91 (1989) 461-466.

[85] E. Cardoso, G. Baume, C. R. Hebd. Seanc. Acad. Sci. Paris 151 (1910) 141-143.

[86] J. Dewar, London Edinb. Dub. Philos. Mag. J. Sci. Ser. 5 18 (1884) 210-216.

[87] A. Leduc, C. R. Hebd. Seanc. Acad. Sci. Paris 148 (1909) 407-410.

[88] IUPAC, J. Phys. Chem. Ref. Data 30 (2001) 701-712.

[89] D.R. Stull, JANAF Thermochemical Tables, second ed., NSRDS-NBS 37, U.S. Department of Commerce, Washington D.C., 1971.

[90] D.R. Stull, Ind. Eng. Chem. 39 (1947) 517-540.

[91] Dortmunder Datenbank, Mixture Properties, Version 6.3.0.384, 2010.

[92] NIST Standard Reference Database 23, Programm REFPROP, Version 9.0, 2010.

[93] E.A. Guggenheim, J. Chem. Phys. 13 (1945) 253-261.

[94] E.J. Clapeyron, L'ecole Polytechnique 14 (1834) 153-190.

[95] J.B. Pedley, J. Rylance, N.P.L. Sussex, Computer Analysed Thermochemical Data. Organic and Organometallic Compounds, University of Sussex, Brighton, 1977.

[96] C. Tsonopoulos, AIChE J. 24 (1978) 1112-1115.

[97] S.D. Hamann, W.J. McManamey, J.F. Pearse, Trans. Faraday Soc. 49 (1953) 351-357.

Table 1
Parameters of the molecular models for Cyanogen and Cyanogen chloride. LJ interaction sites are denoted by the modeled atoms. Electrostatic interaction sites are denoted by dipole or quadrupole, respectively. Coordinates are given with respect to the center of mass in a principal axes system. Orientations of the electrostatic sites are defined in standard Euler angles, where φ is the azimuthal angle with respect to the $x-z$ plane and θ is the inclination angle with respect to the z axis.

interaction site	x	y	z	σ	ϵ/k_B	θ	φ	μ	Q
	Å	Å	Å	Å	K	deg	deg	D	DÅ
Cyanogen									
N	0	0	1.8676	3.3186	35.70				
C	0	0	0.6877	3.5673	28.56				
C	0	0	−0.6877	3.5673	28.56				
N	0	0	−1.8676	3.3186	35.70				
quadrupole	0	0	0			0	0		−9.91
Cyanogen chloride									
Cl	0	0	−1.5824	3.45	240.00				
C	0	0	−0.3989	2.86	19.00				
N	0	0	1.2322	3.37	52.00				
dipole	0	0	0			0	0	2.69	
quadrupole	0	0	0			0	0		−3.87

Table 2
Critical properties of the pure fluids on the basis of present molecular models in comparison to reference data.

Fluid	T_c^{sim}	T_c^{ref}	ρ_c^{sim}	ρ_c^{ref}	p_c^{sim}	p_c^{ref}	Ref.
	K	K	mol/l	mol/l	MPa	MPa	
Cyanogen	384 (4)	397.15-401.45	6.8 (2)	6.62	4.8 (3)	5.92-6.25	[19,85–87]
Cyanogen chloride	446 (4)	449.00	6.9 (2)	6.14	6.0 (4)	5.99	[88–90]

Table 3
Pure substance parameters of the Peng-Robinson EOS, taken from DDB [91] or Refprop [92] or derived from the present simulation results in case of Cyanogen chloride.

substance	T_c	p_c	ω	M
	K	MPa	-	g/mol
Acetone	508.1	4.70	0.309	58.079
Acetonitrile	548.0	4.83	0.321	41.052
Ammonia	405.6	11.28	0.250	17.030
Benzene	562.1	4.89	0.212	78.112
Chlorobenzene	632.4	4.52	0.249	112.56
Chloroform	536.4	5.47	0.216	119.38
Cyanogen	400.0	5.98	0.279	52.035
Cyanogen chloride	449.0	5.99	0.322	61.470
Ethanol	516.2	6.38	0.635	46.068
Hydrogen cyanide	456.8	5.39	0.407	27.030
Methanol	512.6	8.10	0.559	32.042
Toluene	591.7	4.11	0.257	92.138

Table 4
Binary interaction parameter of the molecular models and binary parameter of the Van der Waals one-fluid mixing rule of the Peng-Robinson equation of state as adjusted in the present work.

Mixture	ξ	k_{ij}
Ammonia + Acetonitrile	0.97	−0.015
Acetone + Acetonitrile	1	0.017
Acetonitrile + Chlorobenzene	0.96	0.084
Acetonitrile + Ethanol	0.89	0.071
Acetonitrile + Toluene	0.918	0.081
Benzene + Acetonitrile	1.024	0.075
Chloroform + Acetonitrile	0.99	0.021
Cyanogen + Acetonitrile	1 [a]	−0.225
Cyanogen + Cyanogen chloride	1 [a]	−0.025
Cyanogen + Hydrogen cyanide	1 [a]	−0.125
Cyanogen chloride + Acetonitrile	1 [a]	−0.010
Cyanogen chloride + Hydrogen cyanide	1.023	0.030
Hydrogen cyanide + Acetonitrile	1.02	−0.054
Methanol + Acetonitrile	0.86	0.035

[a] Not adjusted due to lack of experimental data

List of Figures

Fig. 1. Saturated densities of Cyanogen (●) and Cyanogen chloride (■): experimental saturated liquid density [20–22,30,31] (+); DIPPR correlation of experimental data [19] (——). The statistical uncertainties of the present simulation data are within symbol size.
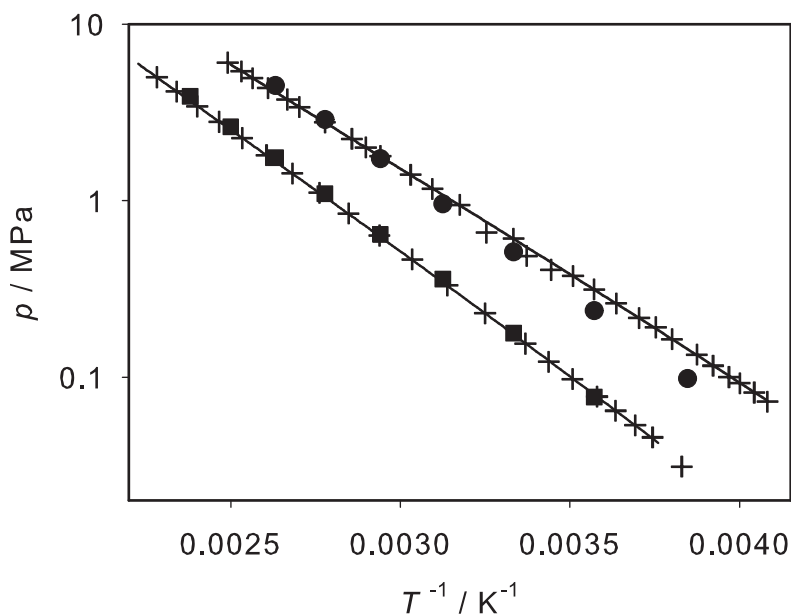

Fig. 2. Logarithmic vapor pressure of Cyanogen (●) and Cyanogen chloride (■): experimental data [21,23–28,33–36] (+); DIPPR correlation of experimental data [19] (——). The statistical uncertainties of the present simulation data are within symbol size.
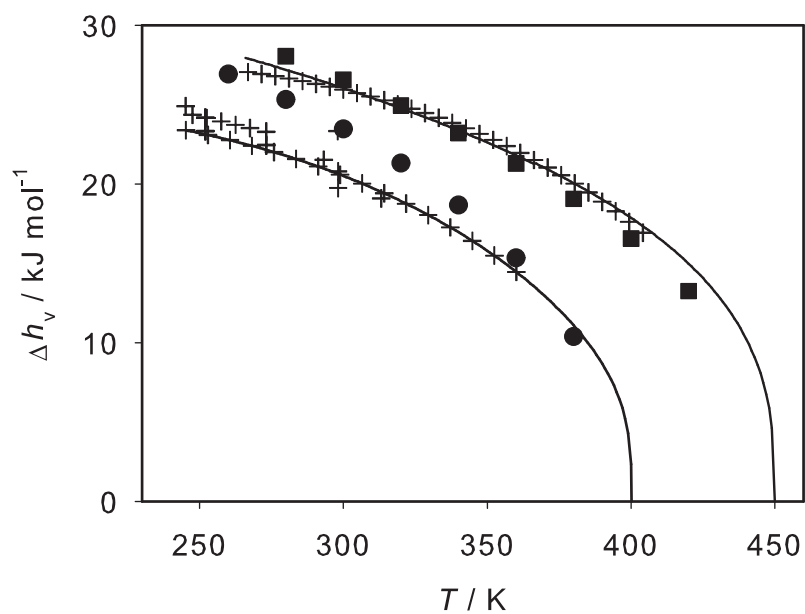
Fig. 3. Enthalpy of vaporization of Cyanogen (●) and Cyanogen chloride (■): experimental data [24,25,94] (+); DIPPR correlation of experimental data [19] (——). The statistical uncertainties of the present simulation data are within symbol size.
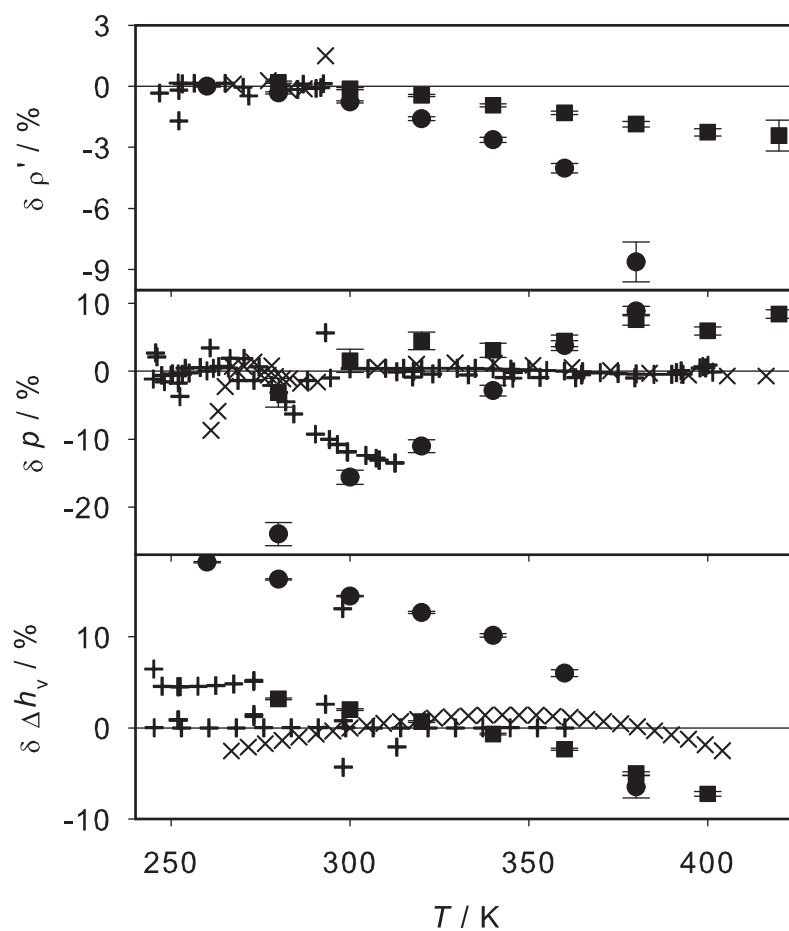
Fig. 4. Relative deviations of vapor-liquid equilibrium properties from correlations of experimental data [19]. Cyanogen: simulation data (●), experimental data [20–28,94] (+); Cyanogen chloride: simulation data (■), experimental data [20,22,30–36,94] (×). Top: saturated liquid density, center: vapor pressure, bottom: enthalpy of vaporization. The error bars indicate statistical uncertainties of the present simulation data.
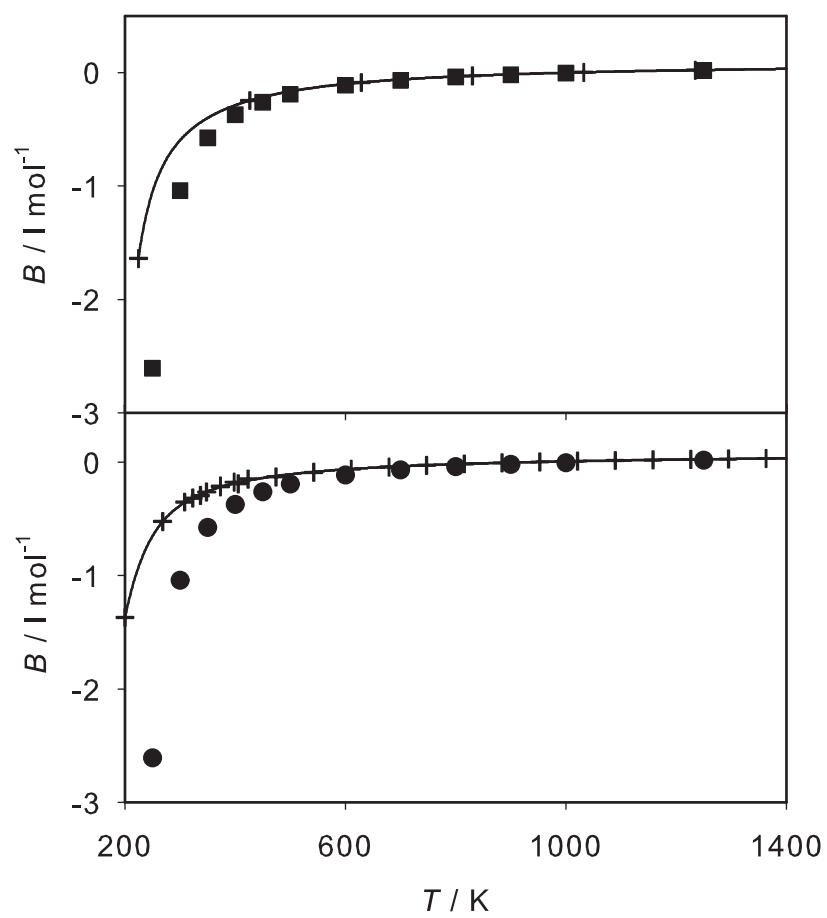
Fig. 5. Second virial coefficient of Cyanogen (●) and Cyanogen chloride (■): data predicted by DIPPR [96,97] (+); DIPPR correlations of predicted data [19] (——).
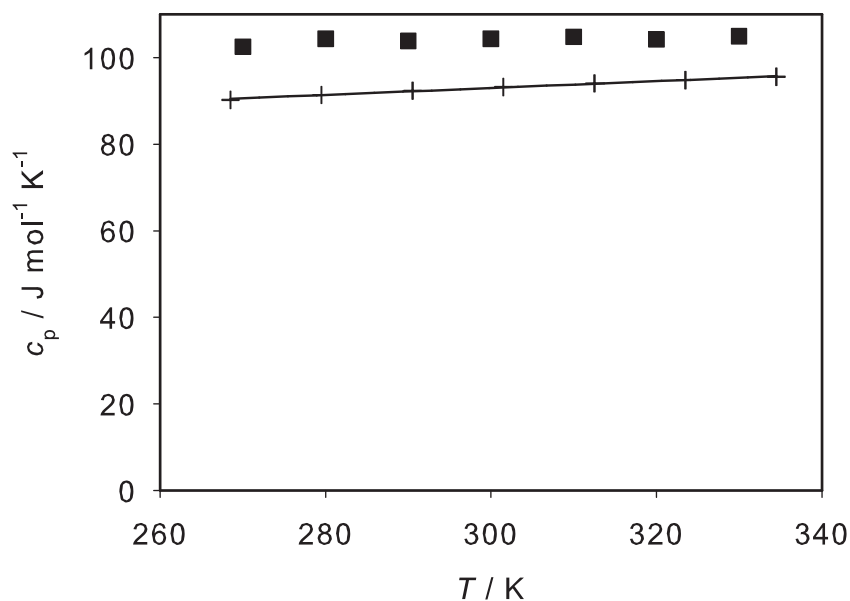
Fig. 6. Isobaric heat capacity of liquid Cyanogen chloride at 0.1 MPa (■): experimental data [32] (+); DIPPR correlation of experimental data [19] (——). The statistical uncertainties of the present simulation data are within symbol size.
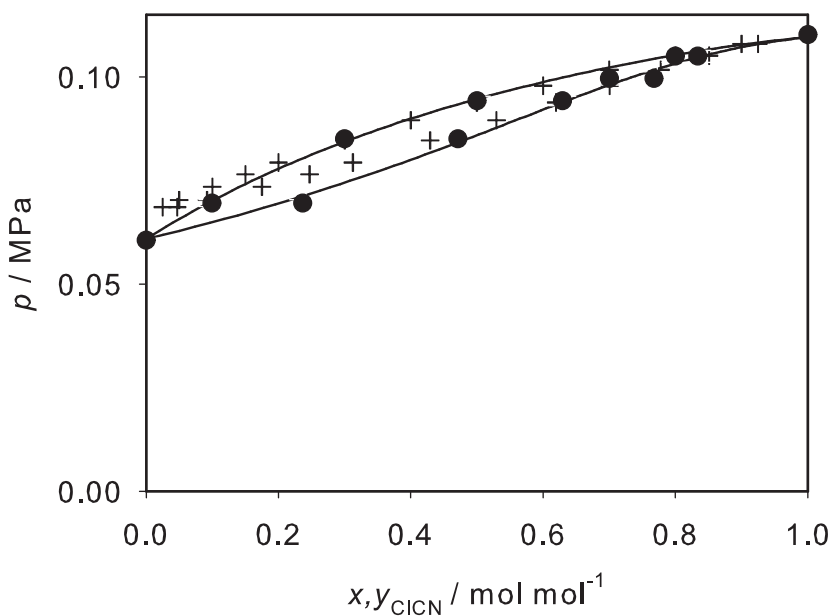
Fig. 7. Isothermal vapor-liquid phase diagram of Cyanogen chloride + Hydrogen cyanide at 288.15 K: present simulation data with $\xi = 1.023$ (●); experimental data by Gordon and Benson [65] (+); Peng-Robinson EOS with $k_{ij} = 0.03$ (——). The statistical uncertainties of the present simulation data are within symbol size.
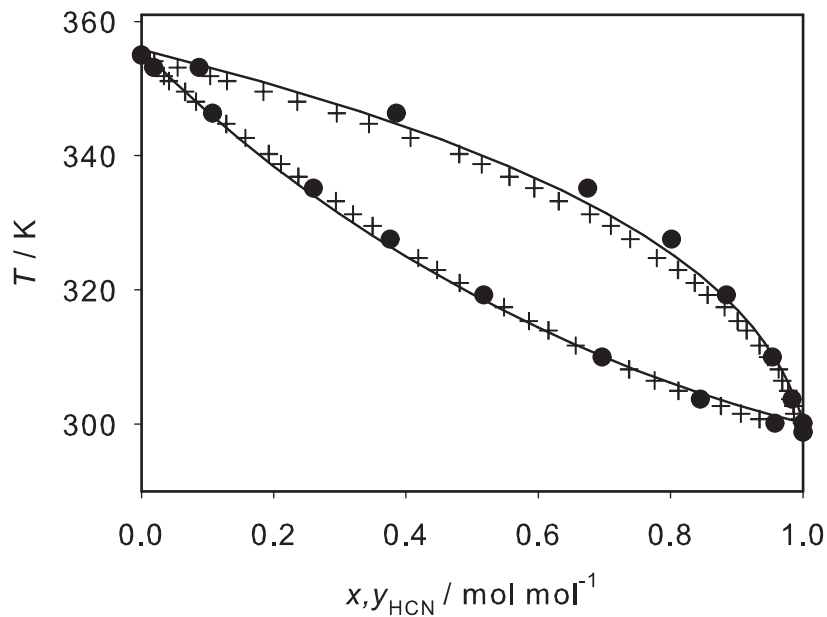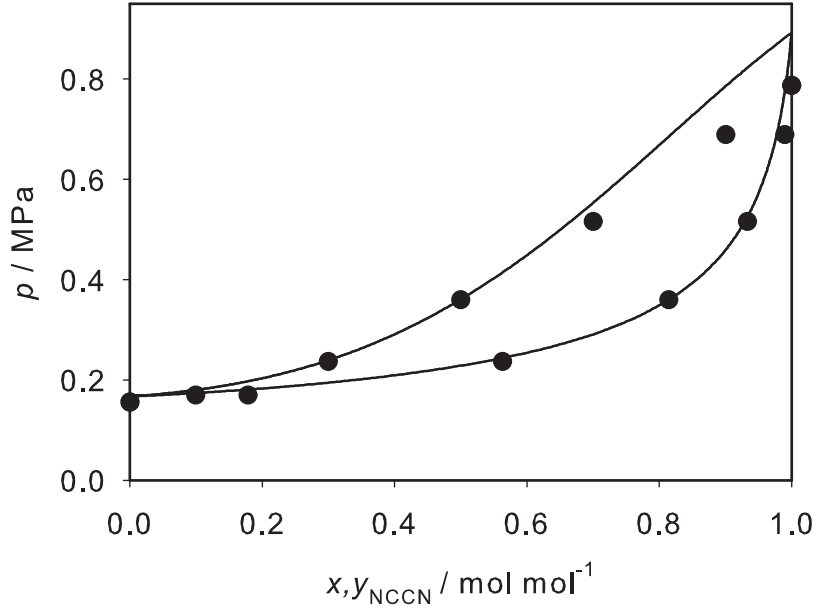
Fig. 8. Isobaric vapor-liquid phase diagram of Hydrogen cyanide + Acetonitrile at 0.10133 MPa: present simulation data with $\xi = 1.02$ ($\bullet$); experimental data by Jiang et al. [66] (+); Peng-Robinson EOS with k_{ij} = -0.054 (———). The statistical uncertainties of the present simulation data are within symbol size.
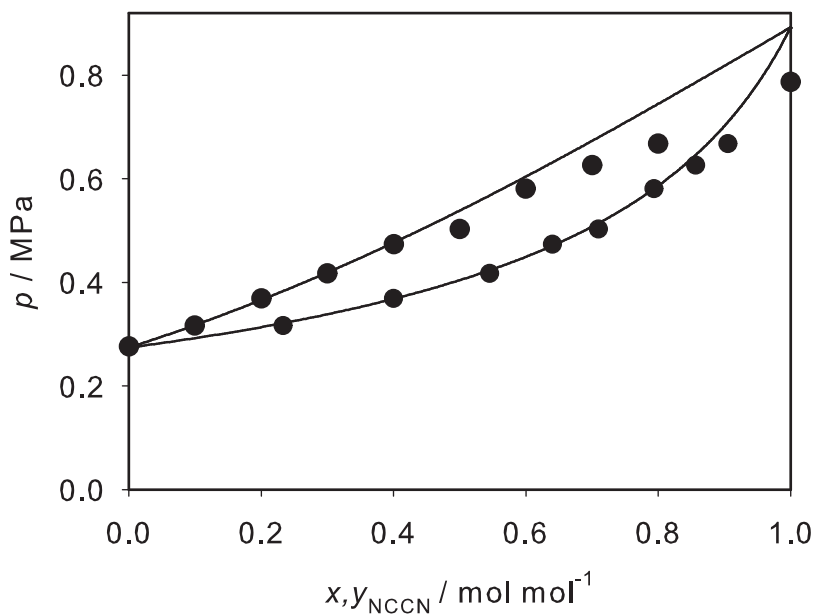
Fig. 9. Isothermal vapor-liquid phase diagram of Cyanogen + Cyanogen chloride at 313.15 K: present simulation data with $\xi = 1$ ($\bullet$); Peng-Robinson EOS with k_{ij} = -0.025 (———). The statistical uncertainties of the present simulation data are within symbol size.
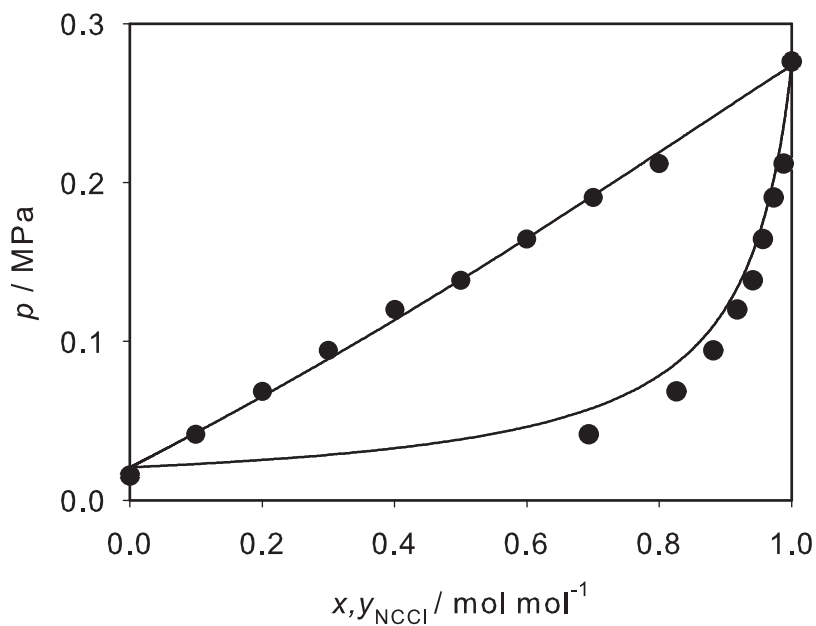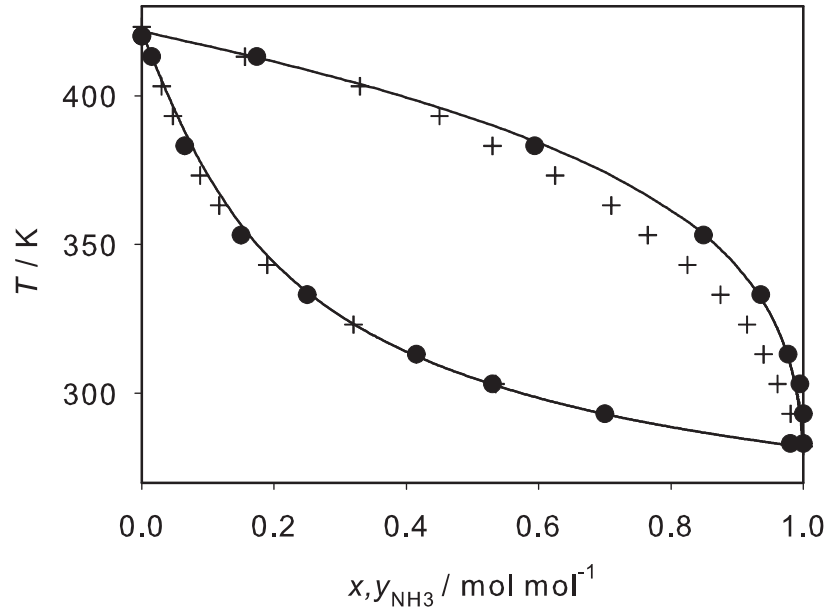
Fig. 10. Isothermal vapor-liquid phase diagram of Cyanogen chloride + Acetonitrile at 313.15 K: present simulation data with $\xi = 1$ ($\bullet$); Peng-Robinson EOS with $k_{ij} = $ -0.01 (——). The statistical uncertainties of the present simulation data are within symbol size.
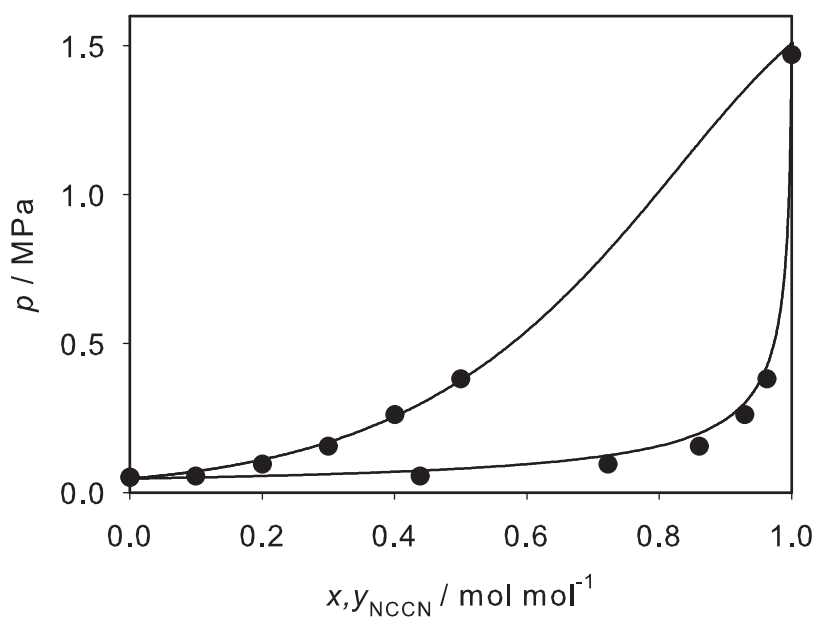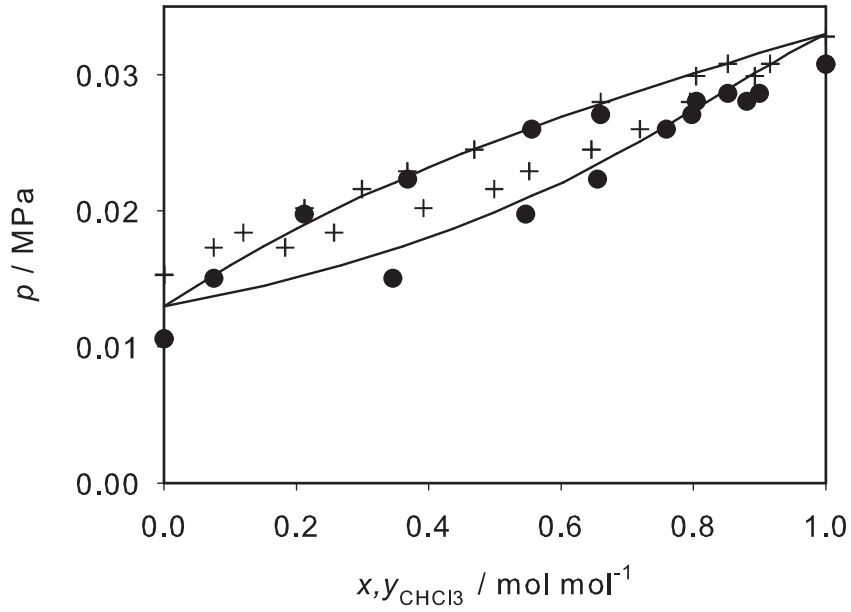

Fig. 11. Isothermal vapor-liquid phase diagram of Cyanogen + Acetonitrile at 333.15 K: present simulation data with $\xi = 1$ ($\bullet$); Peng-Robinson EOS with $k_{ij} = $ -0.225 (——). The statistical uncertainties of the present simulation data are within symbol size.
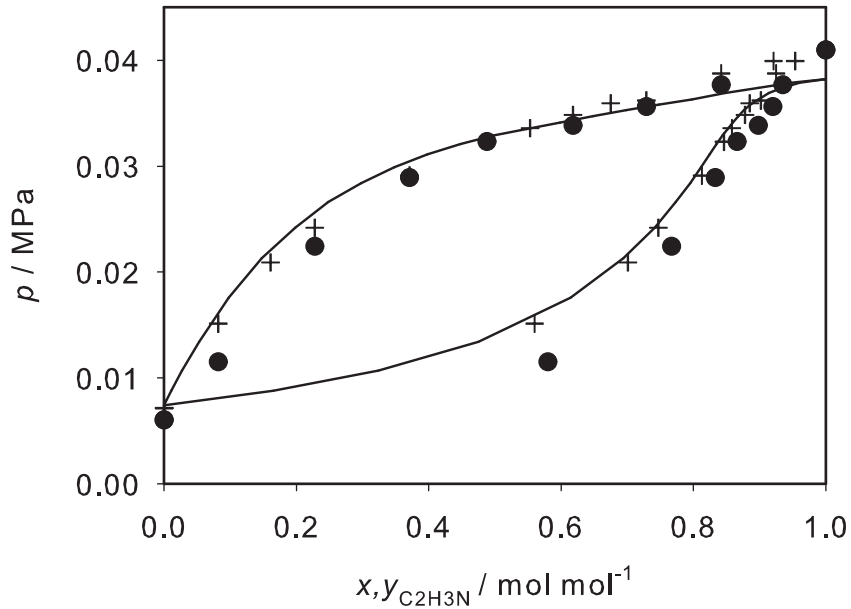
Fig. 12. Isothermal vapor-liquid phase diagram of Cyanogen + Hydrogen cyanide at 313.15 K: present simulation data with $\xi = 1$ (●); Peng-Robinson EOS with $k_{ij} = -0.125$ (——). The statistical uncertainties of the present simulation data are within symbol size.

Fig. 13. Isobaric vapor-liquid phase diagram of Ammonia + Acetonitrile at 0.59 MPa: present simulation data with $\xi = 0.97$ (●); experimental data by Tyvina and Fokina [67] (+); Peng-Robinson EOS with $k_{ij} = -0.015$ (——). The statistical uncertainties of the present simulation data are within symbol size.
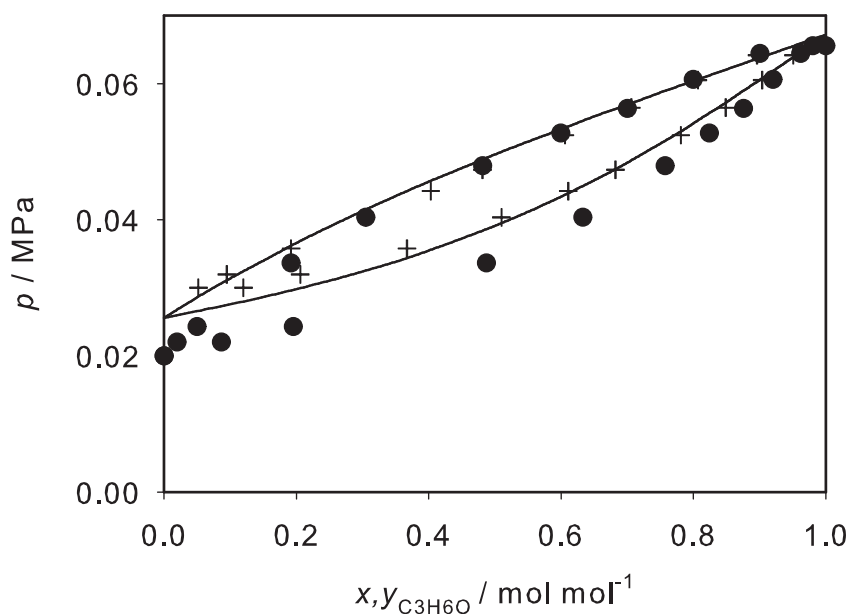
41

Fig. 14. Isothermal vapor-liquid phase diagram of Chloroform + Acetonitrile at 303.15 K: present simulation data with $\xi = 0.99$ (●); experimental data by Lazarte et al. [68] (+); Peng-Robinson EOS with $k_{ij} = 0.021$ (——). The statistical uncertainties of the present simulation data are within symbol size.

Fig. 15. Isothermal vapor-liquid phase diagram of Acetonitrile + Chlorobenzene at 328.15 K: present simulation data with $\xi = 1$ (●); experimental data by Nagata [69] (+); Peng-Robinson EOS with $k_{ij} = 0$ (——). The statistical uncertainties of the present simulation data are within symbol size.

Fig. 16. Isothermal vapor-liquid phase diagram of Acetone + Acetonitrile at 318.15 K: present simulation data with $\xi = 1$ ($\bullet$); experimental data by Brown and Smith [70] (+); Peng-Robinson EOS with $k_{ij} = 0.017$ (——). The statistical uncertainties of the present simulation data are within symbol size.
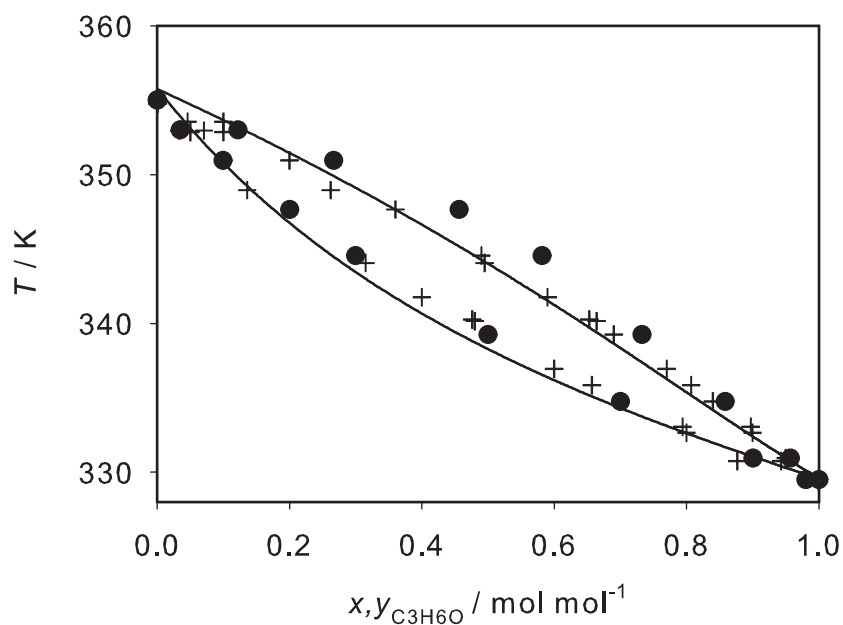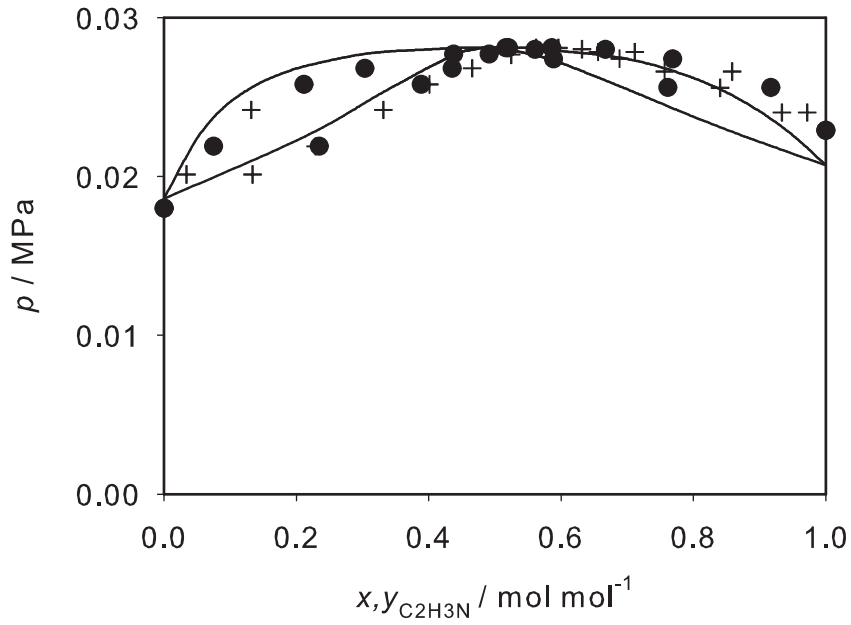

Fig. 17. Isobaric vapor-liquid phase diagram of Acetone + Acetonitrile at 0.10133 MPa: present simulation data with $\xi = 1$ ($\bullet$); experimental data by Gorshkov et al. [71] and Pratt [72] (+); Peng-Robinson EOS with $k_{ij} = 0.017$ (——). The statistical uncertainties of the present simulation data are within symbol size.

43

Fig. 18. Isothermal vapor-liquid phase diagram of Acetonitrile + Ethanol at 313.15 K: present simulation data with $\xi = 0.89$ ($\bullet$); experimental data by Sugi and Katayama [73] (+); Peng-Robinson EOS with $k_{ij} = 0.071$ (——). The statistical uncertainties of the present simulation data are within symbol size.
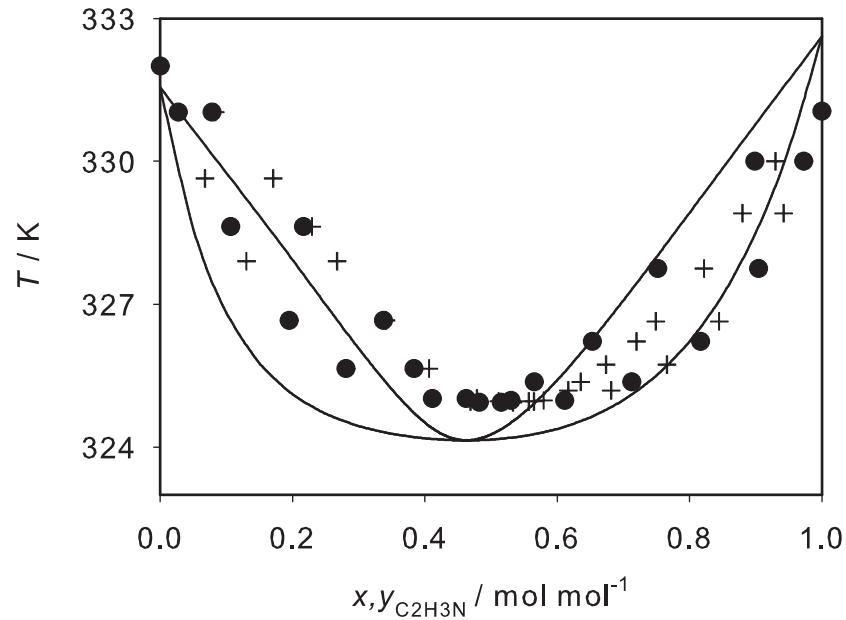

Fig. 19. Isobaric vapor-liquid phase diagram of Acetonitrile + Ethanol at 0.045 MPa: present simulation data with $\xi = 0.89$ ($\bullet$); experimental data by Dohnal et al. [74] (+); Peng-Robinson EOS with $k_{ij} = 0.071$ (——). The statistical uncertainties of the present simulation data are within symbol size.
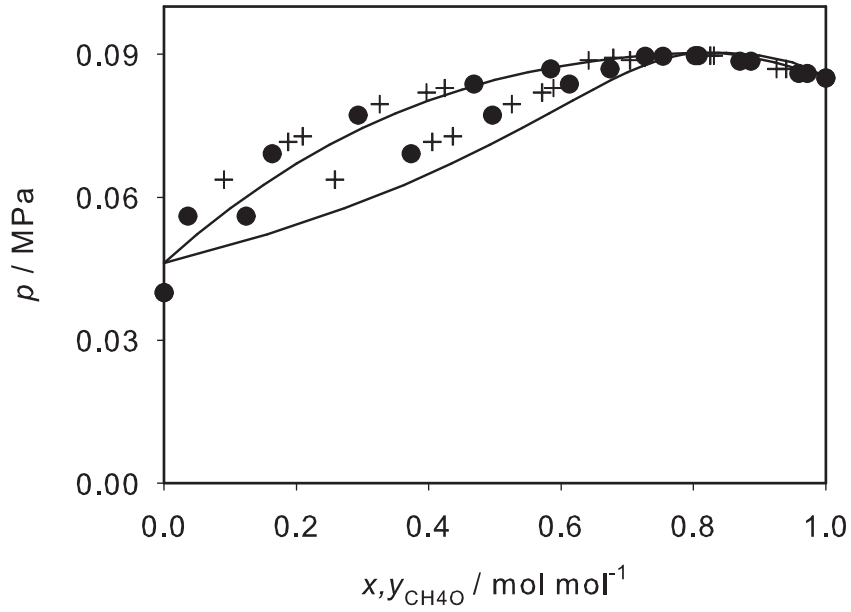
Fig. 20. Isothermal vapor-liquid phase diagram of Methanol + Acetonitrile at 303.15 K: present simulation data with $\xi = 0.86$ ($\bullet$); experimental data by Dohnal et al. [75] (+); Peng-Robinson EOS with $k_{ij} = 0.035$ (——). The statistical uncertainties of the present simulation data are within symbol size.
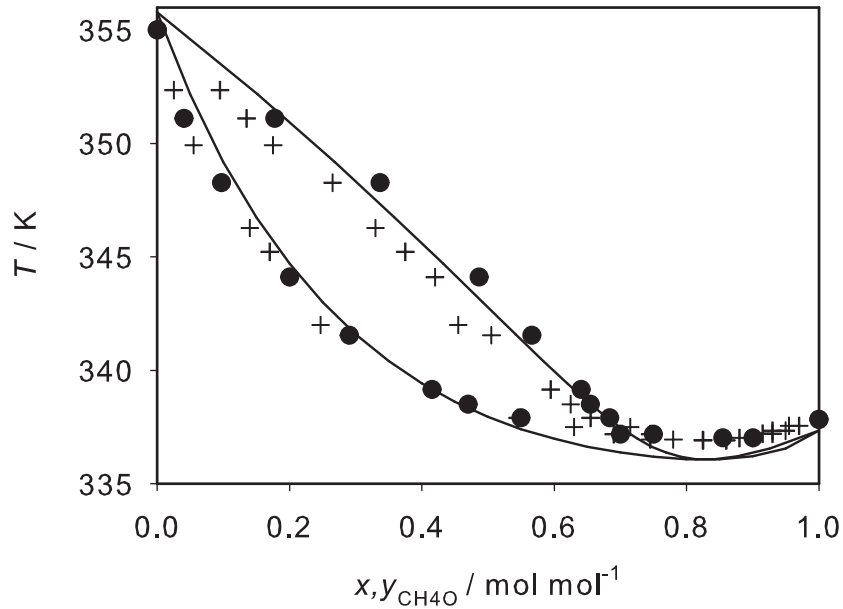

Fig. 21. Isobaric vapor-liquid phase diagram of Methanol + Acetonitrile at 0.10133 MPa: present simulation data with $\xi = 0.86$ ($\bullet$); experimental data by Tamir and Wisniak [76] (+); Peng-Robinson EOS with $k_{ij}=0.035$ (——). The statistical uncertainties of the present simulation data are within symbol size.
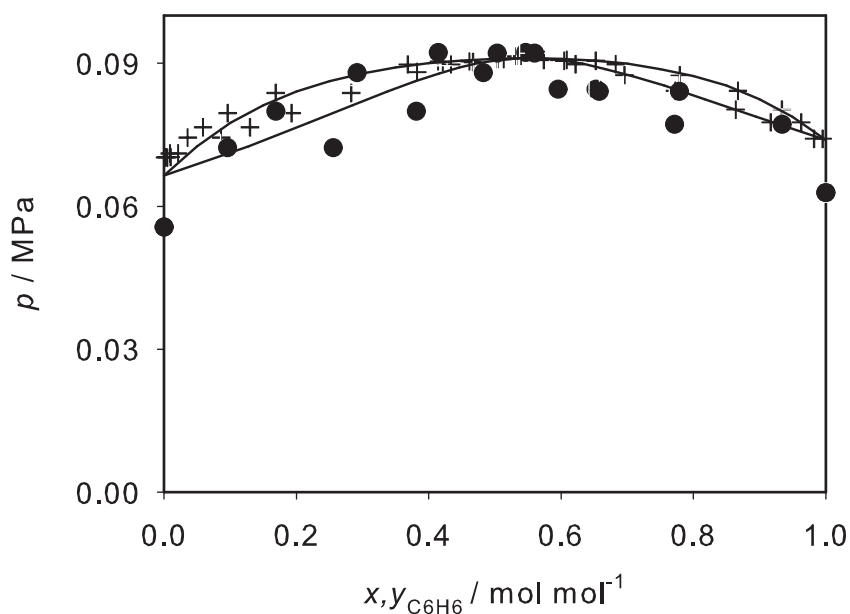
Fig. 22. Isothermal vapor-liquid phase diagram of Benzene + Acetonitrile at 343.15 K: present simulation data with $\xi = 1.024$ (●); experimental data by Monfort [77] (+); Peng-Robinson EOS with $k_{ij} = 0.075$ (———). The statistical uncertainties of the present simulation data are within symbol size.
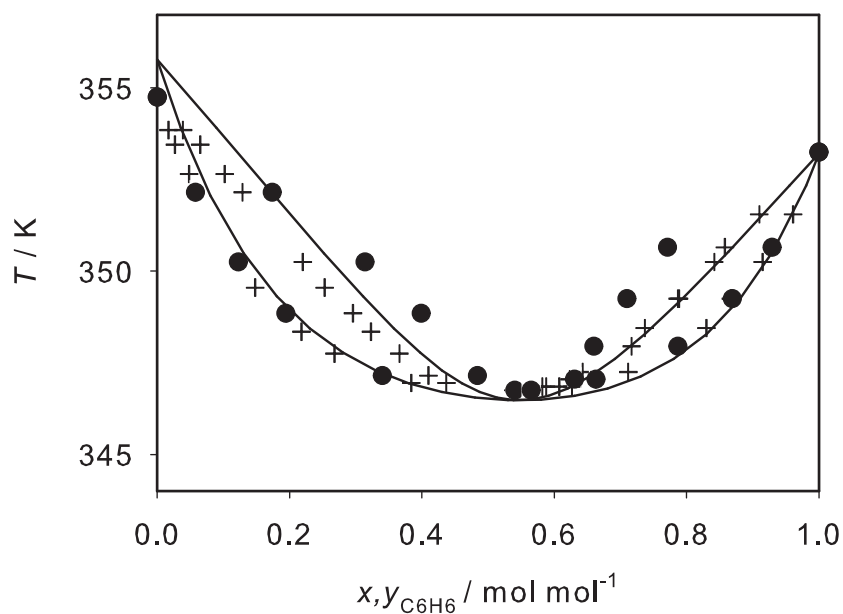

Fig. 23. Isobaric vapor-liquid phase diagram of Benzene + Acetonitrile at 0.1013 MPa: present simulation data with $\xi = 1.024$ (●); experimental data by Di Cave and Mazzarotta [78] (+); Peng-Robinson EOS with $k_{ij} = 0.075$ (———). The statistical uncertainties of the present simulation data are within symbol size.
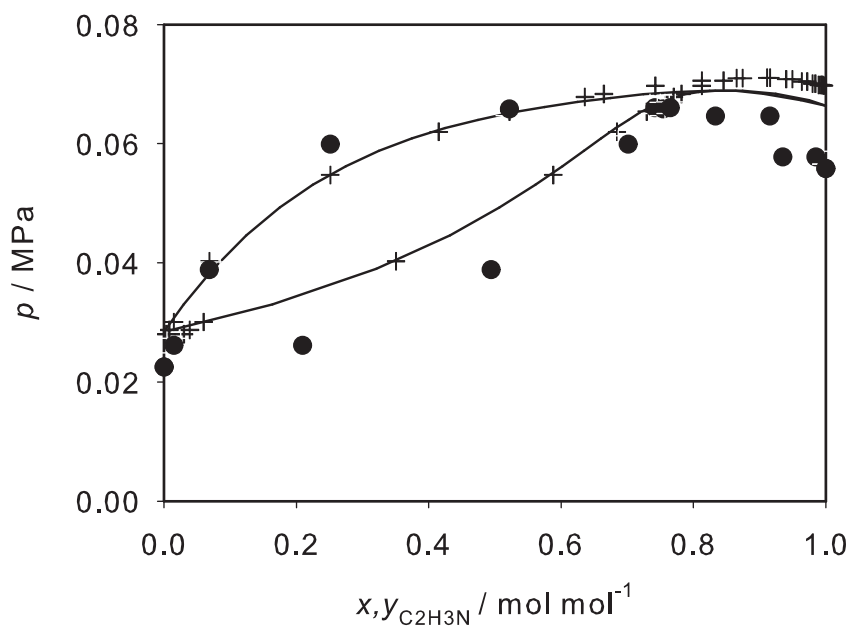
Fig. 24. Isothermal vapor-liquid phase diagram of Acetonitrile + Toluene at 343.15 K: present simulation data with $\xi = 0.918$ (●); experimental data by Monfort [77] (+); Peng-Robinson EOS with $k_{ij} = 0.081$ (——). The statistical uncertainties of the present simulation data are within symbol size.
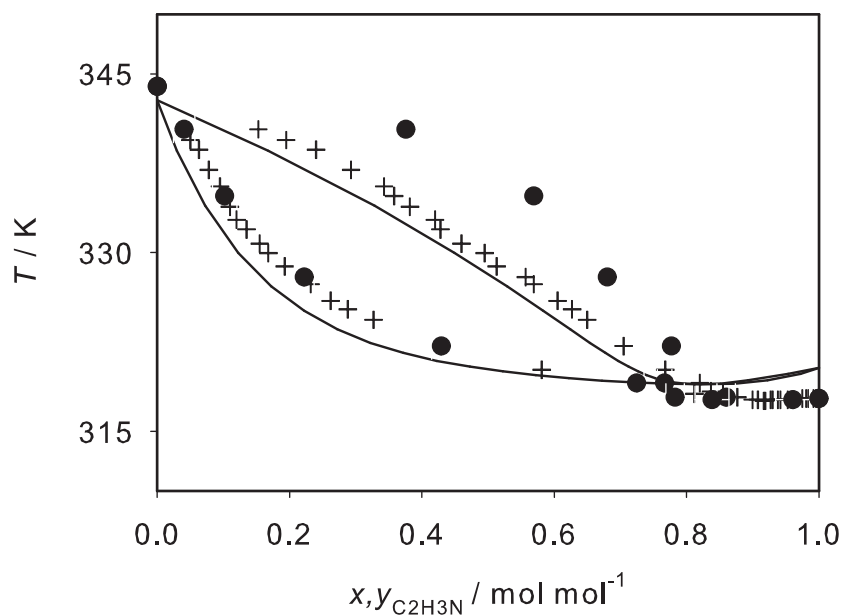

Fig. 25. Isobaric vapor-liquid phase diagram of Acetonitrile + Toluene at 0.028 MPa: present simulation data with $\xi = 0.918$ (●); experimental data by Di Cave and Mazzarotta [78] (+); Peng-Robinson EOS with $k_{ij} = 0.081$ (——). The statistical uncertainties of the present simulation data are within symbol size.